

Available online at www.sciencedirect.com

Applied Surface Science



Revision

1 Transport properties of water molecules confined between
2 hydroxyapatite surfaces: A Molecular dynamics simulation
3 approach
4

5 Muthuramalingam Prakash^{a,b}, Thibault Lemaire^{a*}, Devis Di Tommaso^c,
6 Nora de Leeuw^d, Marius Lewerenz^e, Matthieu Caruel^a, Salah Naili^a
7

8
9 ^a *Université Paris Est, Laboratoire de Modélisation et Simulation Multi-Echelle, UMR 8208, CNRS, 94010 Créteil, France*

10 ^b *SRM Research Institute and Department of Chemistry, SRM University, Kattankulathur 603203, Tamil Nadu, India*

11 ^c *School of Biological and Chemical Sciences, Queen Mary University of London, Mile End Road, E1 4NS London, United Kingdom*

12 ^d *School of Chemistry, Cardiff University, Main Building, Park Place, Cardiff CF10 3AT, United Kingdom*

13 ^e *Université Paris Est, Laboratoire de Modélisation et Simulation Multi-Echelle, UMR 8208, CNRS, 77454 Marne la Vallée Cedex 2,
14 France*
15
16
17

18 **Abstract**

19 Water diffusion in the vicinity of hydroxyapatite (HAP) crystals is a key issue to describe biomineralization process. In this
20 study, a configuration of parallel HAP platelets mimicking bone nanopores is proposed to characterize the nanoscopic
21 transport properties of water molecules at HAP-water surface and interfaces using various potential models such as
22 combination of the Core-Shell (CS) model, Lennard-Jones (LJ) potentials with SPC or SPC/E water models. When
23 comparing all these potentials models, it appears that the core-shell potential for HAP together with the SPC/E water model
24 more accurately predicts the diffusion properties of water near HAP surface. Moreover, we have been able to put into relief
25 the possibility of observing hydroxyl (OH⁻) ion dissociation that modifies the water structure near the HAP surface.

26
27 **Keywords:** Molecular Dynamics Simulation, HAP-Water Systems, Water Self Diffusion, H-bonding and Hydroxyl Dissociation

28
29 *Corresponding author: Prof. Thibault Lemaire

30 Phone: +33145171572

31 Email: thibault.lemaire@univ-paris-est.fr
32
33

33 1. Introduction

34 Investigation of bone-material is very important to understand the physical properties at bone-material
35 interface [1-5]. Bone mineral phase is made of hydroxyapatite (HAP) [6] which is also present in the teeth
36 enamel. It is often necessary to understand the phenomena occurring at the nanometric scale of the HAP minerals
37 of bone (molecular unit formula $[\text{Ca}_{10}(\text{PO}_4)_6(\text{OH})_2]$) to understand the macroscopic behaviour of this organ [7-
38 9]. During biomineralization, bone-water interface plays an important role in the mechanism of bone
39 reorganization [10]. Thus, the investigation of HAP-water interface materials received widespread attention to
40 understand the chemical, physical and mechanical properties of these materials considering the confinement
41 effect of water near the HAP surface [5,11-13].

42 Similarly, HAP scaffolds are often used in bone repair [14] and is thus the prototype model for the biomaterial
43 adsorption studies [15,16]. The metabolism of bone tissue is characterized by the surface interactions between
44 HAP crystals, cells, water molecules and bridging proteins [17]. Numerous studies have thus been devoted to
45 understand the interaction between HAP surfaces with biomolecules, water, ions, and gases using experimental
46 and theoretical methods [18-25].

47 In particular, it was shown that the interactions between a surface and water molecules may affect the local
48 environment of the interface, modifying the diffusion properties of water molecules which tends to reduce when
49 compared with the bulk phase properties. Several experimental and theoretical reports have been devoted to
50 understand the unusual dynamics of water under confinement [26-32]. Orientation and diffusion mechanisms
51 of water molecules in the vicinity of a surface is still unclear. These reports reveals that polarity, hydrogen
52 bonding (H-bonding) and orientation play a vital role for diffusion of water molecules.

53 Using a molecular dynamics (MD) approach, we were recently able to tackle the question of the interstitial
54 bone fluid flows at the nanoscale [5]. These preliminary results have suggested that mobile water can be
55 observed within HAP pores of the same size as the nanopores measured in bone by Holmes et al. [33]. Based
56 on a molecular dynamics approach involving inter-atomic potentials models for HAP and water systems

57 developed by Leeuw [34], this seminal study was well describing the HAP-water structure at the interface, but
58 was badly adapted to properly describe the diffusive process of confined water [11]. That is why, in this paper,
59 we intend to propose a comparison between different HAP-water models in the perspective of their ability to
60 describe properly the confined diffusion of water in nanopores.

61 The structure of this paper is therefore rather classical since the different water-HAP models are presented
62 in a first Materials and methods section. In particular, the simulation strategy is presented. Then, a section is
63 devoted to present the results and discuss their implications. The peculiar phenomenon of hydroxyl dissociation
64 is also stressed out. Finally, conclusions and prospects are presented.

66 2. Materials and methods

67 2.1. Simulation boxes

68 HAP $[\text{Ca}_{10}(\text{PO}_4)_6(\text{OH})_2]$ is seen as a hexagonal primitive cell with $P6_3/m$ space group, each sphere
69 representing a tetrahedral (PO_4^{3-}) ionic complex. Its natural organization in bone matrix corresponds to a stack
70 of thin micro-plates with dimensions ($L \times l \times e$), where $L=250\text{-}500 \text{ \AA}$, $l=150\text{-}250 \text{ \AA}$ and $e = 25 \text{ \AA}$ [35]. That is
71 why, similarly to the configuration in our previous study [11], the dimensions of parallelepipedic shaped
72 simulation boxes are adjusted to contain $(3 \times 3 \times 4)$ such micro-plates.

73 Due to partial occupancy of OH sites, the orientation of OH groups always protruded away from the surface
74 (i.e. c axis). Moreover, the simulation box contains a water layer whose height may be varied (in the c -axis
75 direction) from 20 \AA to 200 \AA to mimic bone nanopores size. This variation of the water layer thickness is
76 performed by adding or removing water molecules.

77 The position of each atom in the box is given using its Cartesian coordinates (x,y,z) in the orthogonal frame
78 $(\mathbf{e}_1, \mathbf{e}_2, \mathbf{e}_3)$, see Fig. 1. The HAP platelets and water layers constitute the elementary cell which is repeated
79 periodically along the \mathbf{e}_3 axis. The initial coordinates and crystal cell parameters were taken from [36].

2.2. Choice of different intermolecular interactions models

Four types of interatomic potential models were used to describe the interactions in the HAP nanopore-water systems. In the first model hereafter named **CS-water**, the interactions between particles were represented by the core shell interatomic potential developed by de Leeuw and Parker for HAP and water systems [18,37], which includes electronic polarizability via the shell model of Dick and Overhauser. This model was used in our previous studies [11,12]. In this CS-water model the phosphate, hydroxyl group, and oxygen–hydrogen (H_w) bonds are described as the sum of a Morse and a Coulombic potential, the phosphate and water bond angles by a harmonic potential, and non-bonded interactions by Buckingham potentials. This force field makes use of a shell model to represent the oxygen's electronic polarizability in the phosphate and hydroxyl groups, and in the water molecules, in which each oxygen atom consists of both a core and a massless shell connected by a spring.

In the second model, hereafter named **LJ-SPC**, the HAP interactions were described through Lennard-Jones potentials as proposed in [38] while water molecules were described by the SPC model.

The third model (noted **LJ-SPC/E**) is the same as the LJ-SPC except that the SPC/E water model was used instead. This is motivated by the good ability of the simple point charge (SPC/E) model to represent density, radial distribution functions, self-diffusion coefficient for water; and hydrogen-bond dynamics in good agreement with experiment [39-41]. The parameters set for the SPC and SPC/E models can be found in [39,40].

In the fourth model (noted **CS-SPC/E**) the core-shell representation of the HAP mineral of de Leeuw and Parker [37] was combined with the SPC/E water model. This combination of potentials models was validated by activation energy (E_a) calculations [42].

The parameters of these models are listed in Tab. 1 and Supplementary Material (Tables S1 and S2).

2.3. Simulation process

Simulations were performed using the DL POLY molecular dynamics package (version 4.05.1) [43]. Each system was equilibrated in the microcanonical (NVE) ensemble for 50 ps, followed by 100 ps simulations in the isothermal–isobaric (NPT) ensemble, during which the volume was monitored in order to confirm the system reached equilibrium. The Melchionna modification of the Nosé-Hoover algorithm [44] was used with 0.5 ps for the thermostat and barostat relaxation times to maintain an average pressure of 1 atm and an average temperature of 310 K. This choice was made for comparison purpose with our previous work [11], which dealt with human bone environment under in vivo conditions. Thus, pores sizes typically range to classical bone nanopore sizes measured by [33] (between 50 Å and 125 Å).

Production runs in the NPT ensemble were then conducted for at least 2000 ps (i.e. 2 ns). The leap-frog algorithm with a time step of 0.1 fs was used to integrate the equations of motion. Periodic boundary conditions were applied in all directions of the box. The long range electrostatic interactions between the charges of all species were computed using the Smoothed Particle Mesh Ewald (SPME) method with the acceptable relative error of 10^{-6} [45]. The cut-off for calculation of the non-bonding interactions was set to 9 Å.

3. Results and discussion

3.1. Self-Diffusion Coefficient of Water

Our analysis is here focused on describing water diffusion process by depicting the self-diffusion coefficients of water for the different water models for various degrees of confinement, that is to say for various pore sizes.

The self-diffusion coefficients of water molecules D were calculated from the mean-square displacement (MSD) using Einstein's expression:

$$D = \frac{1}{2} \frac{d \langle \langle [r(t) - r(0)]^2 \rangle \rangle}{dt} \quad (1)$$

Here, $r(t)$ corresponds to the position of a particle (water molecule) at time t . The chevrons notation stands for the averaging procedure.

Figure 2 displays the dependence of the self-diffusion coefficient D in terms of pore size H at 310K for the four HAP-water interaction potentials models. Note that the experimental bulk water self-diffusivity is also presented by the green bullet.

As expected, it is found from our calculation that the self-diffusivity of water gradually increases with the pore sizes, whatever be the type of interaction potential model.

Indeed, at 298 K for instance, the bulk water diffusion coefficients for SPC or SPC/E models are 3.85 and $2.3 \times 10^{-9} \text{ m}^2 \cdot \text{s}^{-1}$, respectively [46]. Here, due to the confinement effect, the calculated values are always lower even if the higher temperature should induce an increase in the water molecules mobility. This is due to the strong electrostatic interactions between the HAP surface and water which tend to limit the diffusion process. This will also affect the orientation of water and cooperative effect between surrounding water molecules. A similar trend has also been observed for the other nanoporous materials such as SiO_2 , Fe_3O_4 , CNT, and proteins [46].

When focusing on the differences between the different potentials models, it is first to notice that the LJ-SPC model always provides a much higher value of the water diffusivity than the other potentials models (LJ-SPC/E, CS-SPC/E, CS-water) which give more similar values. This may be explained by the charges of the SPC water model that are lower than the ones of the SPC/E model for instance, causing a faster diffusive transport.

Furthermore, for the small pores ($H < 80 \text{ \AA}$), it appears that the CS-water model of our previous study [11] and the CS-SPC/E present diffusion values that are slightly lower than the LJ-SPC/E predictions. For larger pores, this trend becomes the opposite.

149 It is interesting to note that for small pore sizes (between 20 and 50 Å), the confinement effect on the
150 diffusivity coefficient is linear, whereas for larger pores, this is no more the case. This clearly states that two
151 different kind of diffusion mechanism are possible in structures presenting a HAP-water interface. This may be
152 an evolution from a quasi 1D diffusion process in the narrow pores to anisotropic diffusion of water molecules
153 for lower confinement.

154 Moreover, for the largest simulated pore size value $H = 200 \text{ \AA}$, that is to say for the weakest degree of
155 confinement, it appears that the value obtained from the CS-SPC/E combination potentials model is in very
156 close agreement with the experimental bulk water property. Indeed, a comparison of CS-SPC/E and LJ-SPC/E
157 potentials models gives meaningful insights on the selection of suitable force field for the study of water in
158 contact with HAP surface. For a 200 Å pore size, the CS-SPC/E calculated value of the water self-diffusion,
159 respectively its experimental bulk value, is $2.62 \times 10^{-9} \text{ m}^2.\text{s}^{-1}$, respectively $3.02 \times 10^{-9} \text{ m}^2.\text{s}^{-1}$. This confirms
160 earlier reports that concluded that CS potentials are more suited for describing the HAP-water interface
161 phenomena [2].

162 The role of interstitial fluid flow in bone activity is central through its contribution to the transmission of
163 remodeling signals [47,48]. In particular, nanoscopic flows occurring inside the collagen-apatite matrix of bone
164 may modify the vicinity of the osteocytes [5] which are key actors of bone adaptation. As a result, water
165 diffusion occurring in the vicinity of the HAP crystals is an avenue of research of great interest in bone
166 physiology.

168 *3.2. Observation of Hydroxyl ions dissolution*

169 Due to the strong inductive effect from Ca ion and Ca-O_w bond, water molecules can adsorb/desorb at this
170 interface. This phenomenon plays a role in the OH⁻ ion reorganization on HAP surface, and may locally affect
171 the ionic concentration since we observed hydroxyl dissociation through our simulation with the CS-SPC/E
172 model (see Figures 3 and 4). This anionic specie tends to form multiple H-bonds (acting as a donor as well as

173 acceptor) with the surrounding water molecules. Due to this effect, the translational and rotational mobility of
174 water molecules at this interface become unusual. To describe this phenomenon, atomistic modeling approach
175 can give valuable information to understand the adsorption/desorption and reorganization mechanism in HAP
176 interface. This point is crucial during the biomineralization for instance.

177 It is interesting to note that from our calculations, the hydroxyl dissociation always depends on the pore size.
178 In most of the cases, OH⁻ ions are dissociated and localized only near the surface (see Figure 3) whereas in the
179 case of medium pore sizes (i.e. H=50-70 Å, see Figure 4) we also observed OH⁻ ion slightly moving away from
180 the HAP surface and becoming fully surrounded by water molecules via H-bonding interactions. Notice that H-
181 bonding interactions between OH⁻ ion and water molecules are stronger and shorter compared to the normal
182 water-water H-bonding interactions (see Figure 4).

183 **4. Conclusions and perspectives**

184 We have conducted extensive molecular dynamics simulations of nanopores of HAP containing liquid water
185 in order to determine the effect of confinement on the diffusion properties of water by comparing various
186 combination potentials models. When comparing all these potentials models, it appears that the core-shell
187 potential for HAP together with the SPC/E water model more accurately predicts the diffusion properties of
188 water, the obtained values of the average diffusion coefficients being in good agreement with the experimental
189 data from both bulk and bone-water interfaces [49-51].

190 Due to the strong interactions between water molecules and the functional groups of HAP which are
191 dominant in such confined environment, the diffusion in the nanopore direction is significantly faster than in
192 the direction perpendicular to the HAP surface. As a result the diffusion process depends on H-bonding and
193 orientation of water molecules on the surface. We showed that water molecules mainly interact with calcium
194 ions, reducing its adsorption in the vicinity of the phosphate sites. Thus both Ca ion and OH groups protect the
195 interaction between water and phosphate groups (Fig. S1).

196 Therefore we propose that strong inductive effect from Ca²⁺ and electrostatic interactions between water and

197 surface tend to limit the diffusion process along the z-direction and at the same time induce the water molecules
198 to move along x-direction via H-Bonded interactions. Our study can thus provide the valuable information to
199 understand the mechanism of water movement during the biomineralization process.

200

201

202 **Acknowledgements**

203 The authors are grateful to Université Paris-Est Créteil (UPEC) which supported the French-English
204 consortium. Moreover Muthuramalingam Prakash thanks UPEC for the financial support for his post-doctoral
205 research grant.

206 **References**

- 207 1. Popat, Ketul C., et al. "Influence of engineered titania nanotubular surfaces on bone cells."
208 *Biomaterials* 28.21 (2007): 3188-3197.
- 209 2. de Leeuw, N. H. "Computer simulations of structures and properties of the biomaterial
210 hydroxyapatite." *Journal of Materials Chemistry* 20.26 (2010): 5376-5389.
- 211 3. Lemaire, T., et al. "On the paradoxical determinations of the lacuno-canalicular permeability of bone."
212 *Biomechanics and modeling in mechanobiology* 11.7 (2012): 933-946.
- 213 4. Sansalone, V., et al. "Interstitial fluid flow within bone canaliculi and electro-chemo-mechanical
214 features of the canalicular milieu." *Biomechanics and modeling in mechanobiology* 12.3 (2013): 533-
215 553.
- 216 5. Lemaire, T., et al. "Water in hydroxyapatite nanopores: possible implications for interstitial bone fluid
217 flow." *Journal of biomechanics* 48.12 (2015): 3066-3071.
- 218 6. Slepko, A., and Demkov, A. A.. "First principles study of hydroxyapatite surface." *The Journal of*
219 *chemical physics* 139.4 (2013): 044714.
- 220 7. Yoon, Y. J., and Cowin, S. C. "The estimated elastic constants for a single bone osteonal lamella."
221 *Biomechanics and modeling in mechanobiology* 7.1 (2008): 1-11.

- 222 8. Sansalone, V., et al. "Nanostructure and effective elastic properties of bone fibril." *Bioinspired,*
223 *Biomimetic and Nanobiomaterials* 1.3 (2012): 154-165.
- 224 9. Hellmich, C., and Katti, D. "Multiscale mechanics of biological, bioinspired, and biomedical
225 materials." *MRS Bulletin* 40.04 (2015): 309-313.
- 226 10. Wang, Y., et al. "Water-mediated structuring of bone apatite." *Nature materials* 12.12 (2013): 1144-
227 1153.
- 228 11. Pham, T. T., et al. "Properties of water confined in hydroxyapatite nanopores as derived from
229 molecular dynamics simulations." *Theoretical Chemistry Accounts* 134.5 (2015): 1-14.
- 230 12. Prakash, M., et al. "Anisotropic Diffusion of Water Molecules in Hydroxyapatite Nanopores." *Physics*
231 *and Chemistry of Minerals* (2017) in press.
- 232 13. Chiatti, F., et al. "Water at hydroxyapatite surfaces: the effect of coverage and surface termination as
233 investigated by all-electron B3LYP-D* simulations." *Theoretical Chemistry Accounts* 135.3 (2016):
234 1-15.
- 235 14. Oddou, C., et al. "Hydrodynamics in porous media with applications to tissue engineering." in: K.
236 Vafai (Ed.), *Porous media: applications in biological systems and biotechnology*, CRC Press, Boca
237 Raton, 2011, pp. 75-119.
- 238 15. Kandori, K., et al. "Adsorption of myoglobin onto various synthetic hydroxyapatite particles." *Physical*
239 *Chemistry Chemical Physics* 2.9 (2000): 2015-2020.
- 240 16. Rimola, A., et al. "Ab initio modelling of protein–biomaterial interactions: influence of amino acid
241 polar side chains on adsorption at hydroxyapatite surfaces." *Phil. Trans. R. Soc. A* 370.1963 (2012):
242 1478-1498.
- 243 17. Bagchi, B. "Water dynamics in the hydration layer around proteins and micelles." *Chemical Reviews*
244 105.9 (2005): 3197-3219.
- 245 18. de Leeuw, N. H. "Resisting the onset of hydroxyapatite dissolution through the incorporation of

- 246 fluoride." *The Journal of Physical Chemistry B* 108.6 (2004): 1809-1811.
- 247 19. Almora-Barrios, N., et al. "Density functional theory study of the binding of glycine, proline, and
248 hydroxyproline to the hydroxyapatite (0001) and (0110) surfaces." *Langmuir* 25.9 (2009): 5018-5025.
- 249 20. Sakhno, Y., et al. "Surface hydration and cationic sites of nanohydroxyapatites with amorphous or
250 crystalline surfaces: a comparative study." *The Journal of Physical Chemistry C* 114.39 (2010): 16640-
251 16648.
- 252 21. Bolis, V., et al. "Coordination chemistry of Ca sites at the surface of nanosized hydroxyapatite:
253 interaction with H₂O and CO." *Philosophical Transactions of the Royal Society of London A:
254 Mathematical, Physical and Engineering Sciences* 370.1963 (2012): 1313-1336.
- 255 22. Chiatti, F., et al. "Revealing hydroxyapatite nanoparticle surface structure by CO adsorption: a
256 combined B3LYP and infrared study." *The Journal of Physical Chemistry C* 117.48 (2013): 25526-
257 25534.
- 258 23. Zhao, W., et al. "Surface energetics of the hydroxyapatite nanocrystal–water interface: a molecular
259 dynamics study." *Langmuir* 30.44 (2014): 13283-13292.
- 260 24. Hernandez, S. E. R., et al. "The effect of water on the binding of glycosaminoglycan saccharides to
261 hydroxyapatite surfaces: a molecular dynamics study." *Physical Chemistry Chemical Physics* 17.34
262 (2015): 22377-22388.
- 263 25. Parvaneh, L. S., et al. "Molecular Mechanism of Crystal Growth Inhibition at the Calcium
264 Oxalate/Water Interfaces." *The Journal of Physical Chemistry C* 120.8 (2016): 4410-4417.
- 265 26. Bizzarri, A. R., and Cannistraro S. "Molecular dynamics of water at the protein-solvent interface." *The
266 Journal of Physical Chemistry B* 106.26 (2002): 6617-6633.
- 267 27. Tan, H.-S., et al. "Orientational dynamics of water confined on a nanometer length scale in reverse
268 micelles." *The Journal of chemical physics* 122.17 (2005): 174501.
- 269 28. Su, J., and Guo, H. "Effect of nanotube-length on the transport properties of single-file water

- 270 molecules: transition from bidirectional to unidirectional." *The Journal of chemical physics* 134.24
271 (2011): 244513.
- 272 29. Nguyen, T. X., and Bhatia, S. K. "Some anomalies in the self-diffusion of water in disordered carbons."
273 *The Journal of Physical Chemistry C* 116.5 (2012): 3667-3676.
- 274 30. Das, J., et al. "Anomalous diffusion of water molecules in hydrated lipid bilayers." *The Journal of*
275 *chemical physics* 139.6 (2013): 065102.
- 276 31. Lemaire, T., et al. "Bone water at the nanoscale: a molecular dynamics study." *Computer methods in*
277 *biomechanics and biomedical engineering* 18 sup1 (2015): 1982-1983.
- 278 32. Rani, P., and Biswas, P. "Diffusion of Hydration Water around Intrinsically Disordered Proteins." *The*
279 *Journal of Physical Chemistry B* 119.42 (2015): 13262-13270.
- 280 33. Holmes, J. M., et al. "Gas adsorption and surface structure of bone mineral*." *Biochemistry* 3.12
281 (1964): 2019-2024.
- 282 34. de Leeuw, N. H. "A computer modelling study of the uptake and segregation of fluoride ions at the
283 hydrated hydroxyapatite (0001) surface: introducing a Ca₁₀(PO₄)₆(OH)₂ potential model." *Physical Chemistry Chemical Physics* 6.8 (2004): 1860-1866.
- 284 35. Weiner, S., and Traub, W. "Organization of hydroxyapatite crystals within collagen fibrils." *FEBS*
285 *Lett.* 206 (1986):262–266.
- 286 36. Sudarsanan, K., Young, R.A. "Significant precision in crystal structural details. Holly springs
287 hydroxyapatite." *Acta Crystallogr. Sect. B.* 25 (1969):1534–1543.
- 288 37. de Leeuw, N.H., Parker, S.C. "Molecular dynamics simulation of MgO surfaces in liquid water using
289 a shell-model potential for water." *Phys. Rev. B.* 58 (1998):13901–13908.
- 290 38. Lin, T.-J. "Force field parameters and atomistic surface models for hydroxyapatite and analysis of
291 biomolecular adsorption at aqueous interfaces.", phd thesis, The University of Akron, 2013.
- 292 39. Berendsen, H. J. C., et al. "Interaction models for water in relation to protein hydration." *Intermolecular*
293

- 294 forces. Springer Netherlands, 1981. 331-342.
- 295 40. Berendsen, H. J. C., et al. "The missing term in effective pair potentials." *Journal of Physical Chemistry*
296 91.24 (1987): 6269-6271.
- 297 41. Kropman, M. F. and Bakker, H. J. "Femtosecond mid-infrared spectroscopy of aqueous solvation
298 shells." *J. Chem. Phys.* 2001, 115, 8942–8948.
- 299 42. Di Tommaso, D., et al. "Molecular dynamics simulations of hydroxyapatite nanopores in contact with
300 electrolyte solutions: The effect of nanoconfinement and solvated ions on the surface reactivity and
301 the structural, dynamical and vibrational properties of water." *Crystals* (2017) in press.
- 302 43. Todorov, I.T., et al. "DL POLY 3 (new dimensions in molecular dynamics simulations via massive
303 parallelism)." *J. Mater. Chem.* 16 (2006):1911–1918.
- 304 44. Melchionna, S., et al. "Hoover NPT dynamics for systems varying in shape and size. " *Molec. Phys.*
305 78.3 (1993): 533-544.
- 306 45. Essmann, U., et al. "A smooth particle mesh Ewald method." *The Journal of chemical physics* 103.19
307 (1995): 8577-8593.
- 308 46. van der Spoel, D., et al. "A systematic study of water models for molecular simulation: derivation of
309 water models optimized for use with a reaction field." *The Journal of chemical physics* 108.24 (1998):
310 10220-10230.
- 311 47. Fritton, S.P., and Weinbaum, S. "Fluid and solute transport in bone (flow-induced
312 mechanotransduction)." *Ann. Rev. Fluid Mech.* 41 (2009):347–374.
- 313 48. Lemaire, T., et al. "What is the importance of multiphysical phenomena in bone remodelling signals
314 expression? A multiscale perspective." *J. Mech. Behav. Biomed. Mater.* 4 (2011):909–920.
- 315 49. Mills, R. "Self-diffusion in normal and heavy water in the range 1-45. deg." *The Journal of Physical*
316 *Chemistry* 77.5 (1973): 685-688.
- 317 50. Weingärtner, H. "Self diffusion in liquid water. A reassessment." *Zeitschrift für Physikalische Chemie*

318 132.2 (1982): 129-149.

319 51. Mark, P, and Nilsson, L. "Structure and dynamics of the TIP3P, SPC, and SPC/E water models at 298
320 K." *The Journal of Physical Chemistry A* 105.43 (2001): 9954-9960.

321

322

323
324 **TABLES AND FIGURES**

325 **Tables**

326 Table 1. Potential parameters used in this work for the Lennard-Jones and water models.

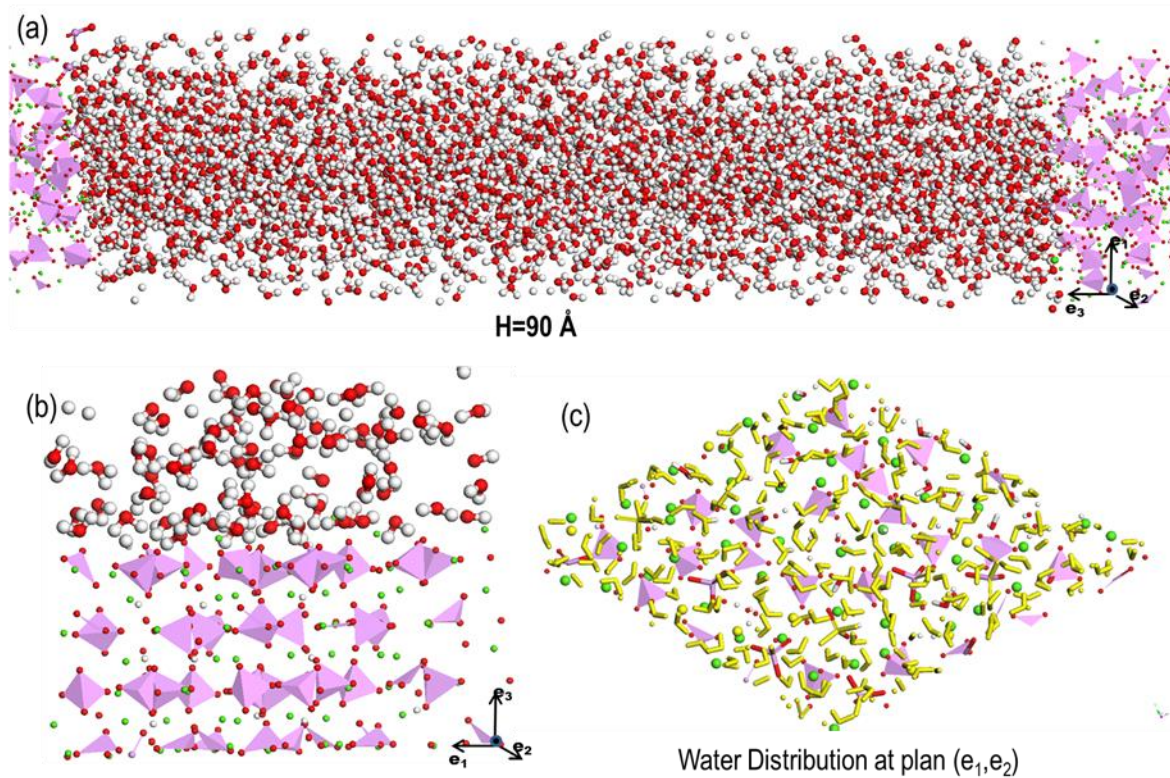
Atomic Partial Charges: (for LJ)		
Atom Types	Charges (e)	
Ca	+1.5	
P	+1.0	
Phosphate Oxygen (O2)	-0.8	
Hydroxy Oxygen (O1)	-1.1	
Hydroxy Hydrogen (H1)	+0.2	
Water Oxygen (Ow)	SPC= -0.82; SPC/E= -0.8476	
Water Hydrogen (Hw)	SPC= +0.41; SPC/E=+0.4238	
Lennard-Jones (LJ) Potential: $U(r) = 4\epsilon \left[\left(\frac{\sigma}{r} \right)^{12} - \left(\frac{\sigma}{r} \right)^6 \right]$		
Ion Pair	ϵ (in kcal/mol)	σ (in Å)
Ca-O1	0.10198	3.5
Ca-O2	0.09539	3.35
O1-O1	0.08	3.7
O1-O2	0.07483	3.55
O2-O2	0.07	3.4
O _w -O1	0.1115	3.433
O _w -O2	0.104298	3.283
O _w -Ca	0.142434	3.233
O _w -O _w	0.1554	3.166
Harmonic Potential: $U(r) = \frac{1}{2}k(r - r_0)^2$		
Ion Pair	k(kcal/(mol.Å ²))	r ₀ (Å)

P-O2	430	1.57
H1-O1	500	0.94
O _w -H _w	1108.2698	1.00
Three-body Potential: $U(\theta) = \frac{1}{2}k(\theta - \theta_0)^2$		
Ion Group	k(kcal/(mol.rad ²))	$\theta_0(^{\circ})$
O2-P-O2	125	109.47
H _w -O _w -H _w	91.5392	109.47

327

328

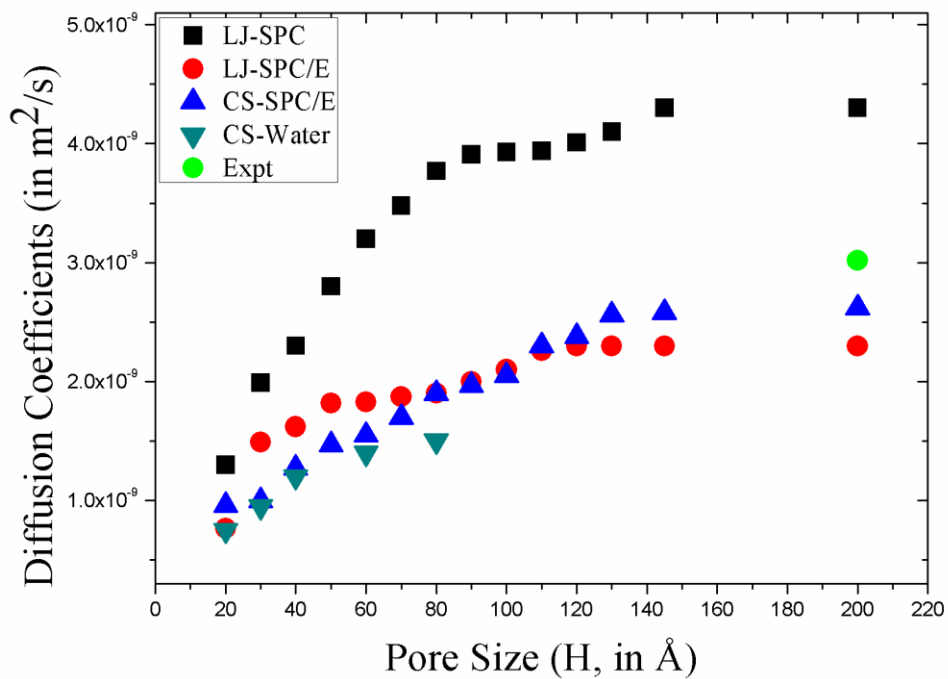
329

330
331**Figures**

332

333 Fig. 1. Water-HAP system (Ca-green, PO_4^{3-} -pink, O-red, H-white): (a) Molecular arrangement of water
334 molecules in a 90 \AA HAP pore; (b) Interaction of water layers with surfaces; (c) Water layer (yellow) adsorbed
335 on the HAP surface.

336



337

338

Fig. 2. Self-diffusion coefficients of water molecules calculated at 310 K for various pore sizes ($H = 20$ to 200 \AA) with different potentials models: LJ-SPC, LJ-SPC/E, CS-SPC/E, CS-water. The experimental diffusion coefficient is also presented.

339

340

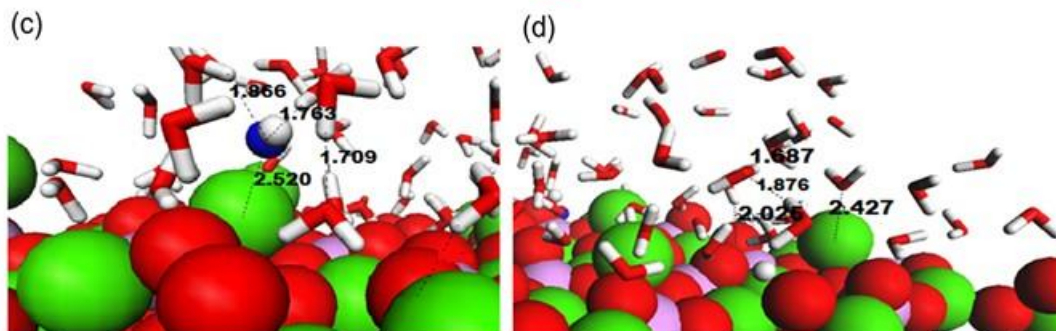
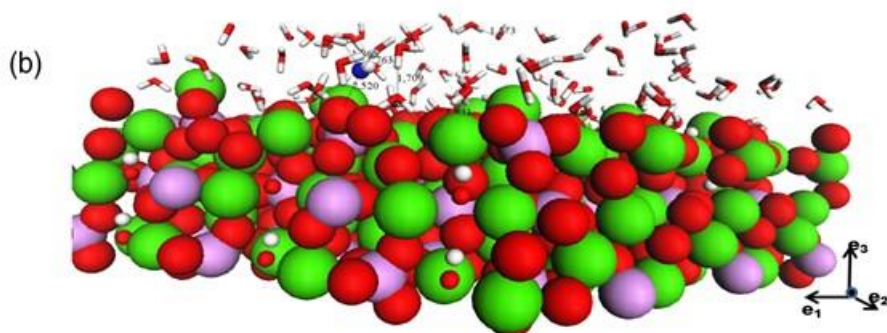
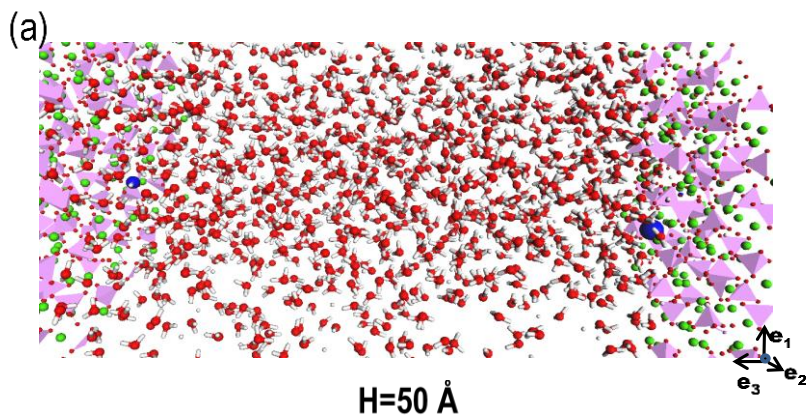
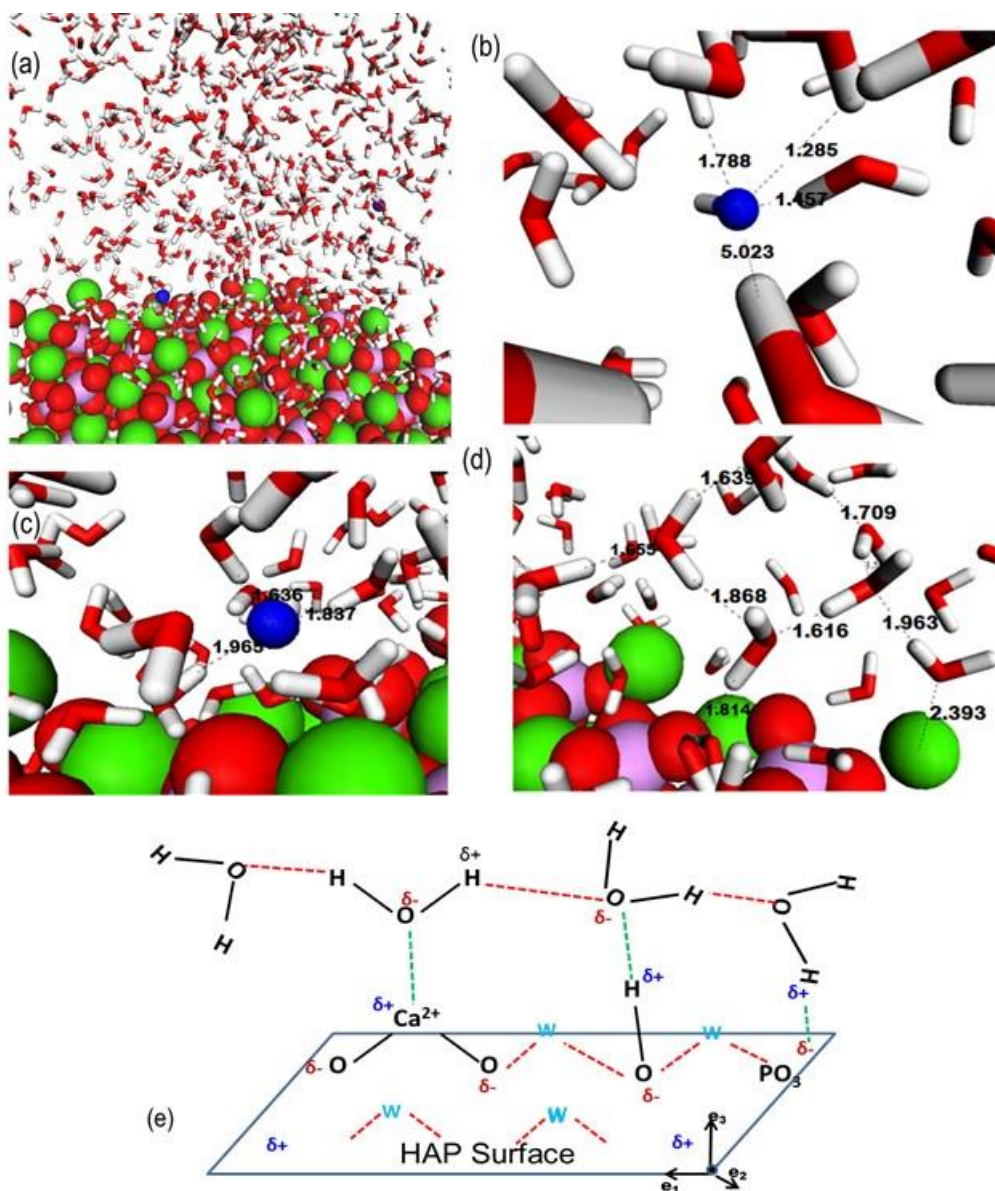


Fig. 3. Hydroxyl ions in HAP-Water system (Ca-green, PO_4^{3-} -pink, O-red, H-white and hydroxyl O-blue): (a) Molecular arrangement of water molecules and OH^- ions in a 50 Å HAP nanopore; (b) Interaction of OH^- ions with HAP-water layers; (c) and (d) shows the close views of H-bonds (distances are in Å) for OH^- -water and water-water, respectively, at the vicinity of HAP interface.



347

348

349

350

351

352

353

Fig. 4. Unusual hydroxyl ion diffusion in HAP-Water system (Ca-green, PO₄³⁻-pink, O-red, H-white and hydroxyl O-blue): (a) Molecular arrangement of water molecules and OH⁻ ions in a 70 Å HAP pore; (b) and (c) Interactions of OH⁻ ion with water molecules near and far away from the HAP surface respectively; (d) H-bonded network between water molecules and Ca²⁺-water interactions (Distances are in Å). (e) Schematic representation of HAP and water adsorption sites through H-bonding at interface.